RSC Advances

RSC Publishing

PAPER

View Article Online
View Journal | View Issue

TEMPO coated Au nanoparticles: synthesis and tethering to gold surfaces†

Cite this: *RSC Advances*, 2013, **3**, 5979

Olga Swiech, Renata Bilewicz and Elżbieta Megiel*

Received 29th November 2012,
Accepted 8th February 2013

DOI: 10.1039/c3ra23106b

www.rsc.org/advances

Gold nanoparticles covered by derivatives of 2,2,6,6-tetramethylpiperidine-1-oxyl (TEMPO) with well-defined coverage and narrow size distribution were synthesized and self-assembled on the gold electrode. The TEMPO nanoparticle-coated electrode was characterized using STM and AFM. The kinetics of oxidation of the nitroxide radicals attached to the nanoparticles was evaluated based on cyclic voltammetry measurements. The TEMPO–nanoparticle modified electrode was found more efficient in electrocatalytic oxidation of benzyl alcohol than the electrode modified with a monolayer of TEMPO molecules directly bound to the gold surface.

1 Introduction

Nitroxides, in particular TEMPO (2,2,6,6-tetramethylpiperidine-1-oxyl), are well-known oxidation catalysts with a number of applications in organic synthesis, including oxidation of primary and secondary alcohols, sulfides and organometallic compounds.[1–3] Of particular interest is the reaction of oxidation of alcohols to carbonyl compounds, catalyzed by oxoammonium cations formed during the oxidation of nitroxides with primary oxidants, *e.g.* hypochlorite, or O_2 with active metal catalysts (Ru^{2+}, Mn^{2+}/Co^{2+} and Cu^{+}).[4] It was reported that the TEMPO radical can be used in catalytic aerobic oxidation of alcohol to aldehydes and ketones in ionic-liquids.[5] Recently TEMPO and its derivatives have found industrial applications in the production of medicines and others speciality chemicals.[6]

The immobilization of homogeneous catalysts facilitates separation and allows easy catalyst recycling. TEMPO radicals were anchored earlier to solid supports, *e.g.* polymers,[7] silica,[8] zeolites[9] and recently multi-walled carbon nanotubes.[10] Tanaka *et al.* reported electrooxidation of selected primary and secondary alcohols with nitroxyl radicals immobilized on silica gel in aqueous solution $NaHCO_3$/NaBr with platinum electrodes which can be applied to enantioselective oxidation of *meso*-1,4-diol affording optically active γ-lactone.[11,12]

Tokuda *et al.*[13] reported the preparation of a glassy carbon rotating electrode modified with TEMPO radical for 4-methoxybenzyl alcohol electrooxidation. On the basis of the electrochemical behavior of the TEMPO modified electrode they proposed a mechanism for electrooxidation of alcohol in the presence of 2,6-lutidine as reaction medium. It was found that the rate-determining step is the decomposition of an intermediate formed from the oxoammonium cation, 4-methoxybenzyl alcohol and 2,6-lutidine acting as a proton acceptor. The presence of 2,6-lutidine is essential for the alcohol electrooxidation to proceed at a reasonable rate.[13]

In the last years interest in the application of metallic nanoparticles in the preparation of new effective and recyclable catalysts has increased rapidly.[14] Contrary to typical heterogeneous catalysts, nanoparticles can be soluble in many solvents thus can act homogeneously and at the same time their activity is very high under mild conditions because of their large surface area.[14] Gold nanoparticles (AuNPs) are especially convenient in such applications due to their high stability, relatively easy preparation and easy introduction of functional groups.[15] The colloidal methods of synthesis are the most commonly used in the preparation of gold nanoparticles.[16] They are based on the reduction of gold salts dissolved in organic solvents in the presence of surface capping ligands which prevent aggregation of the particles by electrostatic and/or physical repulsion.[16] For water soluble gold nanoparticles with *ca.* 20 nm diameter, the Turkevitch method of citrate reduction of $HAuCl_4$ is a favorable approach.[17] Brust and co-workers two-phase procedure involving tetraoctylammonium bromide as a phase-transfer reagent is usually employed for thiol-stabilized gold nanoparticles.[18] This procedure has been applied as the starting point in many experiments using different types of sulfur containing capping ligands such as di and trithiols, xanthates, resorcinarene tetrathiols and disulfides.[19]

Application of disulfides in gold and silver nanoparticles preparation was proposed in the literature as a promising way to obtain mixed monolayers with homogeneous distribution of the functional groups.[20] The mechanism of disulfides adsorption on the gold surface has been repeatedly discussed in the

Faculty of Chemistry, University of Warsaw, Pasteura 1, 02-093 Warsaw, Poland. E-mail: emegiel@chem.uw.edu.pl

† Electronic supplementary information (ESI) available: ESI MS analysis of DiSS, TG, UV, IR, XPS, FTIR analyses of the obtained AuNPs. See DOI: 10.1039/c3ra23106b

literature.[21] Ionita *et al.*[22] reported a place-exchange reaction of stable radical-functionalized disulfide on Au nanoparticles monitored using the EPR technique. They proved a zero-order process with respect to the disulfide concentration, indicative of a dissociative exchange mechanism. Schőnherr and Ringsdorf[23] proved the sulfur–sulfur bond cleavage of the disulfide in the reaction with the gold surface in the studies of unsymmetrical disulfides.

Nitroxide functionalized gold nanoparticles have been prepared earlier in a two-step synthesis with the first step involving the two-phase procedure proposed by Brust and co-workers[18] and a place-exchange reaction of the ligands on the AuNPs as the next step.[24,25] In the place exchange reactions only a small number of nitroxyl radicals replaced the alkanethiols on the AuNP surface and a large excess of incoming ligand should be used.[26] Additionally, the two-phase procedure is limited to non-polar and weakly polar ligands and persistent contamination of isolated products with residual phase transfer agent (tetraoctylammonium bromide) took place.[27] The one-phase procedure was also tried and was carried out in a water–methanol system with a variety of water soluble ligands.[28,29] For the ligands soluble in organic solvents, the anhydrous THF one-phase route was proposed with the very strong reductive agent lithium triethylborohydride.[30] Employing very strong reductive agents causes, however, the reduction of many functional groups during the synthesis. Rowe *et al.*[31] described a one-phase synthesis of thiolate monolayer-protected gold nanoparticles in anhydrous THF with using $LiBH_4$ as the reductive agent. Theato and co-workers[32] prepared functional gold nanoparticles in a two-phase synthesis using disulfides with polar groups as stabilizing ligands in the mixture of ethyl acetate and water with $NaBH_4$ as reductive agent. Under these mild reducing conditions the carboxyl and ester groups survived.

Schätz *et al.*[33] reported the synthesis of graphene-coated nanobeads functionalized by TEMPO radicals and their high activity for the selective oxidation of primary and secondary alcohol. However, the procedure of the described material preparation seems rather complicated.

We described earlier a method of binding the nitroxide functionalized gold nanoparticles obtained in the two-phase mode with a gold electrode through Au–ON< interactions. In this system gold nanoparticles were covered by a mixture of ligands (thiols and nitroxides).[34] Now we report the synthesis of gold nanoparticles covered only by nitroxides, according to a simple one-phase procedure and their application in the preparation of a new type of catalyst for selective alcohol oxidation easy removal from the reaction medium. The obtained nitroxide coated gold nanoparticles were immobilized on the gold electrode surface by means of a 1,9-nonanedithiol linker (Scheme 1). Monolayers obtained in this method should be more stable than prepared by Au–ON< interactions. This is caused by instability of the Au–ON< binding at the potential of catalysis. Cyclic voltammetry was performed for the AuNPs covered electrode and the kinetics of the electrode process of the TEMPO/$TEMPO^+$ couple were evaluated. The modified electrode was applied for electrocatalytic oxidation of benzyl alcohol to aldehyde in acetonitrile,[35] and the catalytic efficiency of the AuNPs nanostructured gold electrode was compared with that of a TEMPO–SH monolayer directly self-assembled on the gold surface.

2 Experimental section

2.1 Materials

$HAuCl_4 \cdot 4H_2O$ in a solution of 30% HCl, and all other solvents were purchased from Sigma–Aldrich. Bis[2-(4-oxy-2,2,6,6-tetramethylpiperidine 1-oxyl)ethyl] disulfide (DiSS) was synthesized according to the procedure described in the literature.[36]

Milli-Q ultrapure water (resistivity 18.2 MΩ cm^{-1}) was used during the preparation of the modified electrodes.

2.2 Preparation of TEMPO covered AuNPs

In a common procedure, 0.3 ml of solution of $HAuCl_4$ (430 μmol) was mixed with 120 ml of ethyl acetate (p.a.); next 300 mg of DiSS (579 μmol) was added (Au : S = 1 : 2.6) and the mixture was stirred under a stream of argon. After 10 min a freshly prepared solution of $NaBH_4$ in methanol (0.274 g in 70 ml, 7.2 mmol) was added slowly during half an hour, under vigorous stirring and a stream of argon. The mixture turned from yellow to dark brown. Next, the solution was stirred under argon atmosphere for 24 h at room temperature. After this time the mixture was washed with deionized water (3 × 100 ml), the organic phase was evaporated to *ca.* 5 ml and precipitated by the addition of *n*-hexane (150 ml). The freshly obtained black precipitate was sonicated in hexane for 1 min and centrifuged (5 min, 15 000 rpm). The solid product was dissolved in THF and then precipitated with hexane. The procedure of dissolving AuNPs in THF and precipitating in hexane was repeated three times until no traces of free ligands were found. The absence of impurities was confirmed by TLC. The obtained solid was dried under vacuum at 40 °C. The dark brown solid (49.9 mg, yield *ca.* 45%) was soluble in most common organic polar solvents, *e.g.* methanol, ethanol, acetone, THF, chloroform, acetonitrile. The solutions were stable and no sedimentation process was observed even after several months.

2.3 Techniques

Transmission Electron Microscopy (TEM) observations were carried out using a JEM 1400 JEOL Co. microscope, at 120 kV acceleration voltage. The samples were obtained by casting the ethanol solution onto a carbon coated nickel microgrid (200 mesh) and air-dried overnight. SEM-EDS spectroscopy measurements were carried out with a scanning electron microscope JEOL-JSM-5600 equipped with a energy dispersive X-ray spectrometer OXFORD Link-ISIS-300.

Thermogravimetric measurements (TG) were performed using a DuPont 951 thermobalance (precision ±0.4%; minimal mass 0.02 mg) coupled with a DuPont 9900 thermal analyzer.

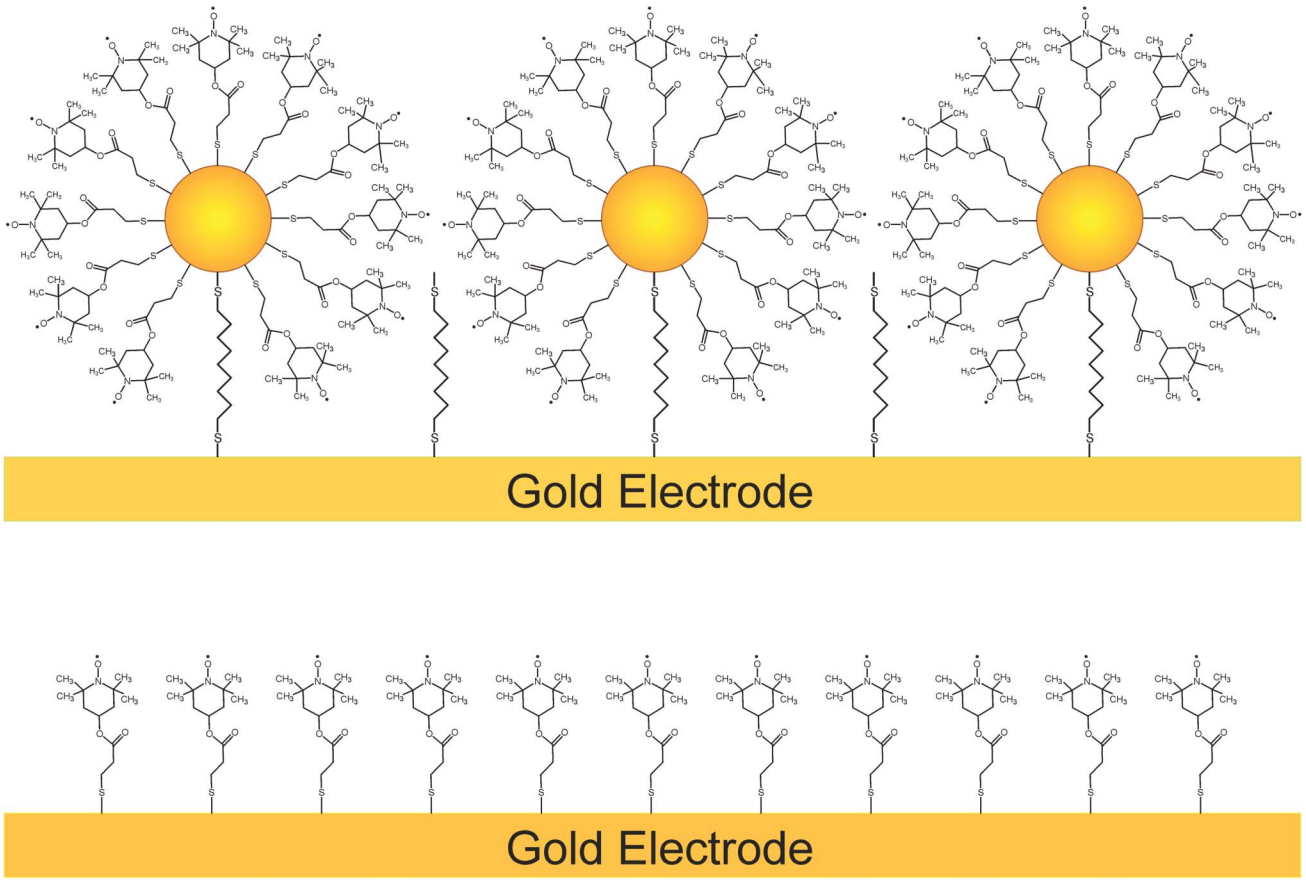

Scheme 1 A schematic presentation of TEMPO nanoparticles (above) and TEMPO–SH monolayer modified gold electrodes (below).

Elemental analysis was performed using a CHNS analyzer model Vario EL III Elementar Analysen systeme GmbH.

Electron Paramagnetic Resonance (EPR) measurements were carried out at room temperature in acetone solution with an X-band (9.3 GHz) using a Miniscope MS200 spectrometer (Magnettech GmbH, Berlin, Germany). Modulation frequency was 100 kHz.

X-Ray photoelectron spectroscopy (XPS) measurements were done using a VG ESCALAB 210 electron spectrometer equipped with an Al Kα source (1486.6 eV). XPS data were calibrated using the binding energy of Au 4f7/2 = 84.0 eV as the internal standard.

Electrochemistry. Voltammetry measurements were performed using a PGSTAT Autolab (Eco Chemie BV, Utrecht, Netherlands) or a CHI 750B potentiostat (CH Instrument, Austin, USA). All electrochemical experiments were done in a three-electrode arrangement with platinum foil as the counter, silver/silver chloride (Ag/AgCl) (BAS) as the reference electrode, and an Au disc (BAS, 1.5 mm diameter) as the working electrode. The supporting electrolyte solution was 0.1 M tetrabutylammonium hexafluorophosphate (TBAHFP) in anhydrous acetonitrile (ACN). Where needed, Milli-Q ultrapure water (resistivity 18.2 MΩ cm^{-1}) was used. The solutions were deaerated using argon and room temperature was maintained.

Scanning tunneling microscope (STM) images were taken under ambient conditions using a Nanoscope IIIa (Digital Instruments, Santa Barbara, CA) and commercially available Pt–Ir tips.

Atomic force microscope (AFM) imaging was performed in the air in ambient conditions using a PicoPlus 5500 AFM (Agilent). The images were taken in alternating current mode (AC-AFM) at a scan rate of 2.0 nm s^{-1} using silicon probes (PPP-NCST, Nanosensors, Switzerland) with an average force constant of 7.4 N m^{-1} and a resonant frequency of 160 kHz.

Preparation of electrode surfaces modified with TEMPO nanoparticles and TEMPO-SH monolayer. Gold disc electrodes (BAS) were polished mechanically with 1.0, 0.3 and 0.05 μm alumina powder on a Buehler polishing cloth. After thorough washing with water, the electrodes were placed in the ultrasound for 10 min in water solution. Next, the substrates were cleaned electrochemically in 1 M NaOH by holding at −1.5 V for 60 s and scanning 10 times within the potential range −1.5 V to 1 V. Finally, they were cleaned in 0.5 M H_2SO_4 solution by cycling the potential in the range −0.2 V to 1.6 V until the characteristic curve for a gold electrode was obtained.[37] The pre-cleaned electrodes were used as the substrates for the deposition of the 1,9-nonanedithiol/butanethiol mixed monolayer from ethanol solution (ratio 1 : 1) for 24 h. The surface concentration of 1,9-nonanedithiol monolayer, calculated from desorption experiments, showed a well-covered monolayer without double adsorption of 1,9-nonanedothiols. Following washing with pure acetone (⩾99.9%) they

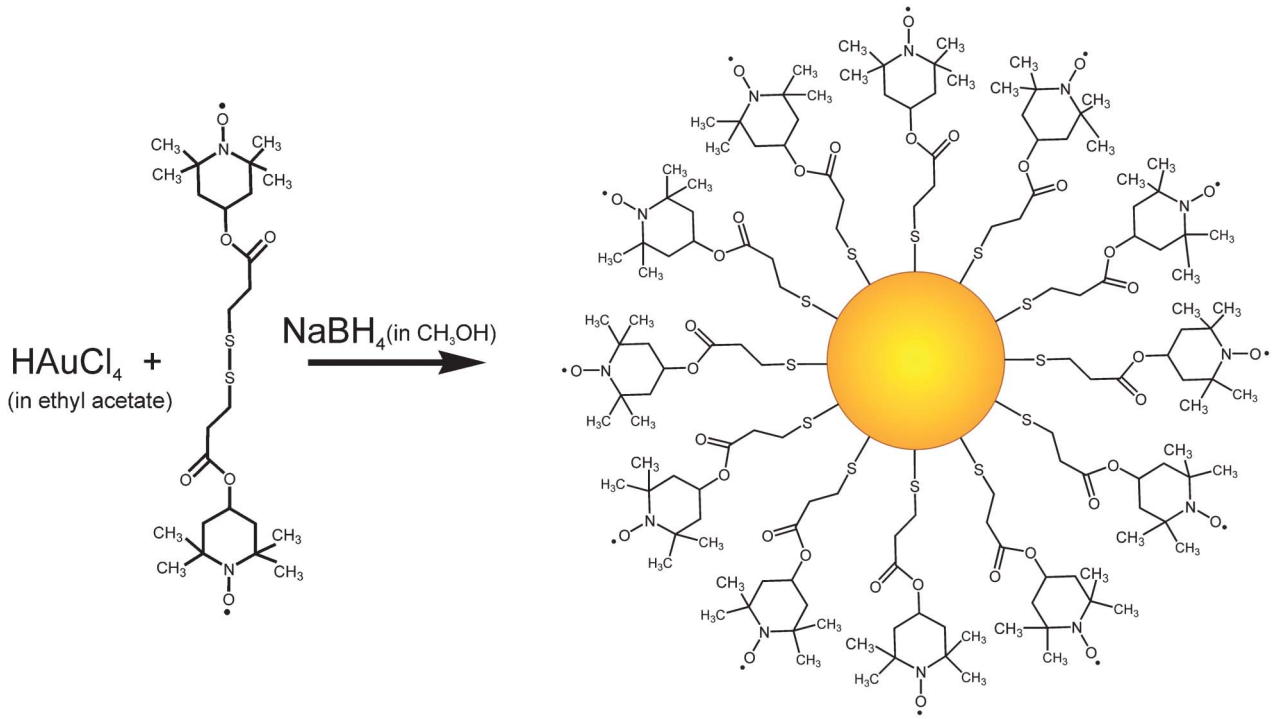

Scheme 2 Synthetic route of the AuNPs preparation.

were immersed in an acetone solution of TEMPO nanoparticles (1 mg ml^{-1}) for 24 h. Finally, the electrodes were washed with acetone and anhydrous acetonitrile, and used in experiments. The idealized structure of the TEMPO NPs modified electrode is shown at Scheme 1. For TEMPO-SH monolayer deposition, the pre-cleaned electrodes were immersed in 5 mM bisnitroxide disulfide (DiSS) solution in acetonitrile for 24 h in the absence of oxygen, then rinsed with acetonitrile and used for further experiments.

3 Results and discussion

3.1 Characterization of AuNPs

AuNPs were obtained in a one-phase procedure using bisnitroxide disulfide as stabilizing ligand, ethyl acetate as reaction medium and methanol as solvent for $NaBH_4$ according to Scheme 2.

The results of our FTIR spectroscopy studies confirm the mechanism proposed in the literature involving cleavage of the disulfide bond during adsorption of disulfide on the gold surfaces (see ESI†).

Fig. 1A and 1B show the TEM image and the size distribution histogram of the obtained nanoparticles, respectively. Clearly, nanoparticles of the size of approximately 2 nm in diameter (2.5 $\pm$ 0.50 nm) and relatively narrow distribution are uniformly dispersed.

Table 1 shows the elemental composition of the gold nanoparticles obtained, determined from EDS, XPS, TG and elemental analysis. With the exception of results from EDS analysis, the composition shows excellent agreement with the expected atomic molar ratio. It should be mentioned that EDS analysis allows identification of the elements in the sample and accurate elemental composition determination is rather limited.

The presence of characteristic functional groups in the obtained AuNPs was confirmed using X-ray photoelectron spectroscopy XPS. The photoemission spectrum of the N(1s) line is shown in Fig. 2. This broad signal was deconvoluted into two peaks at 399.2 and 401.1 eV binding energy, respectively, both with a full width at half maximum (FWHM) of 2.2 eV. The first signal could be attributed to the nitrogen of the nitroxide group NO• according to the literature data (398.9 eV, FWHM = 2.1 eV;[38] 400.6 eV, FWHM = 1.2 eV[39]). The shoulder observed at 401.1 eV shifted by 2.1 eV to higher binding energies can be assigned to a shake-up satellite[40] involving N–O bands in analogy to those observed earlier for

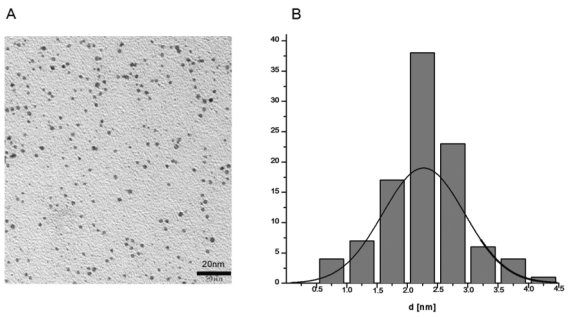

Fig. 1 A) TEM image of the obtained AuNPs and B) their size distribution histogram.

Table 1 The composition of the gold nanoparticles obtained from different methods

	% of weight			
	EDS[a]	XPS[a]	Elemental analysis[b]	TG
Gold	67.3	63.2		76.9
Sulfur	6.87	4.94	3.30	
			3.01	
Nitrogen	2.85	1.91	1.28	
			1.20	
Oxygen	3.24	6.65		
Carbon		23.3	15.33	
			15.30	
Hydrogen			2.13	
			2.14	
Molar ratio Au : S	1.8 : 1	2.08 : 1	3.78 : 1[c]	
Molar ratio:	S : N : O	S : N : O : C	S : N : C : H	
Obtained	1 : 1.1 : 1.1	1 : 0.9 : 2.7 : 12.6	1 : 0.9 : 12.3 : 20.6	
Calculated[d]	1 : 1 : 3	1 : 1 : 3 : 12	1 : 1 : 12 : 21	

[a] Calculated on the basis of atomic %. [b] Data were collected for two samples. [c] From elemental and TG analysis. [d] On the basis of ligand composition.

thin films of TEMPO derivatives on the solid support.[23] The remaining characteristic signals obtained in the XPS spectra are shown in the ESI.†

The EPR spectrum of the obtained AuNPs (Fig. 3) shows a typical three-line spectral pattern of a nitroxide free radical in the fast motion regime overlapping a single broad line with a small amplitude. This broad line probably results from the averaging of a number of EPR signals of groups of radicals close enough to each other on the Au nanoparticle surface to undergo exchange interactions. Also the line width broadening can be ascribed to intermolecular interactions between radicals close to each other.

3.2 Cyclic voltammetric behavior of the gold electrode modified with TEMPO nanoparticles

Cyclic voltammograms obtained for the gold electrode modified with TEMPO covered gold nanoparticles are shown in Fig. 4. The reversible redox peaks centered at *ca.* 0.838 V were ascribed to the redox processes of the TEMPO/TEMPO$^+$ couple. The peak separation of the redox wave was *ca.* 20 mV (at scan rate 1 V s^{-1}), so the anodic and cathodic peaks were nearly mirror images of one another. The electrochemical response at each of the modified electrodes became almost constant after the voltammetric measurement was repeated 15 times and the differences between the anodic peak currents on first and 15th voltammograms were less than 8%. The anodic peak currents exhibited a linear relationship *vs.* potential sweep rate over the range between 10 mV s^{-1} and 1 V s^{-1}. Values of surface concentrations calculated from the area under the TEMPO oxidation peak were equal to $(4.8 \pm 0.45) \times 10^{-10}$ mol cm^{-2} reflecting the high density of the TEMPO groups on the gold electrode. AFM images confirmed that the electrode surface is densely and uniformly packed with TEMPO nanoparticles with only few aggregates (Fig. 5). For comparison, the surface concentration of the TEMPO group for the TEMPO-SH monolayer on the gold electrode was estimated to be much lower, $(1.72 \pm 0.35) \times 10^{-10}$ mol cm^{-2}.

3.3 Kinetics of electron transfer in the TEMPO/TEMPO$^+$ redox system immobilized on the gold electrode

The standard rate constants, k of the electrode processes of TEMPO nanoparticles and TEMPO-SH immobilized on the electrode surface were calculated from the cyclic voltammograms using the Laviron equation:[41,42]

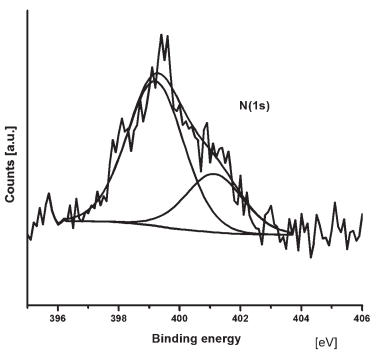

Fig. 2 XPS spectrum of the N(1s) electrons of TEMPO covered AuNPs.

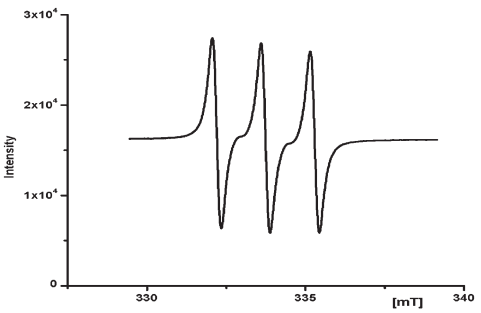

Fig. 3 EPR spectrum at 293 K of TEMPO covered AuNPs in acetone solution.

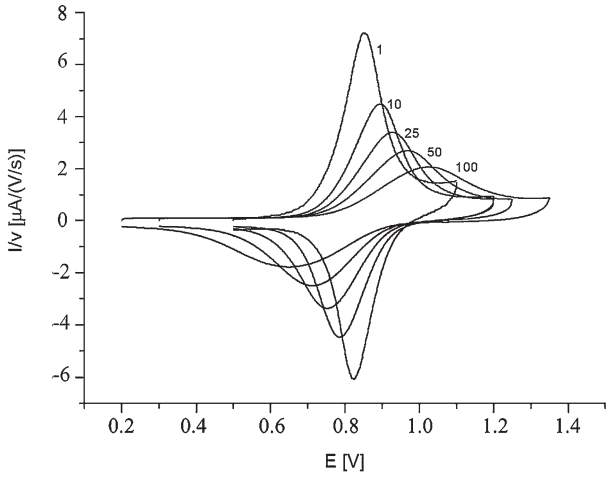

Fig. 4 Cyclic voltammograms of 1,9-nonaneditiol monolayer covered with TEMPO nanoparticles in 0.1 M TBAHFP in ACN. The current is normalized by scan rate (μA/(V s^{-1})). Scan rates (V s^{-1}) are shown in the figure.

$$k = \frac{\alpha \cdot n \cdot F \cdot v_c}{R \cdot T} = \frac{(1-\alpha) \cdot n \cdot F \cdot v_a}{R \cdot T} \quad (1)$$

The scan rate corresponding to the intersection point of the two asymptotes, $v_a = v_c$ is obtained from Fig. 6A and 6B. The transfer coefficient α was obtained by measuring the variation of the peak potential with the scan rate. A plot of E_p *versus* log*v* yields two straight lines with slopes equal to $2.3RT/(1\text{-}\alpha)nF$ and $2.3RT/\alpha nF$ for anodic and cathodic peaks. The scan rate corresponding to the intersection point of the two asymptotes, $v_a = v_b$ is obtained from Fig. 6. For TEMPO-SH monolayer, the electron transfer rate constant, k and electron transfer coefficients α were calculated to be 165 $\pm$ 18 s^{-1} and 0.61 $\pm$ 0.02, respectively.

For the system based on TEMPO nanoparticles, the values of the electron transfer rate constant and transfer coefficient were equal to k = 106 $\pm$ 18 s^{-1}, α = 0.66 $\pm$ 0.07. The smaller electron transfer rate constants for the TEMPO NPs covered electrode may be due to longer alkyl chains in the 1,9-nonanedithiol than in the TEMPO-SH molecule and the less efficient electron transport between the TEMPO molecule

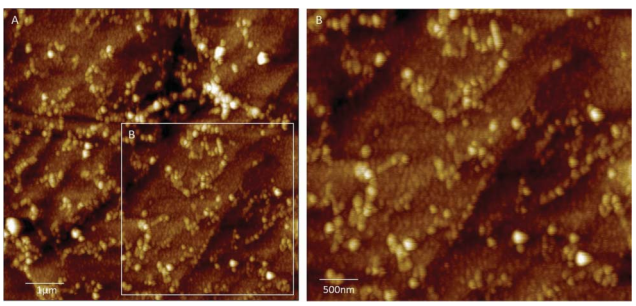

Fig. 5 AFM images of the gold electrode coated with a monolayer of 1,9-nonanedithiol and TEMPO nanoparticles. Nanoparticles deposition time: 24 h.

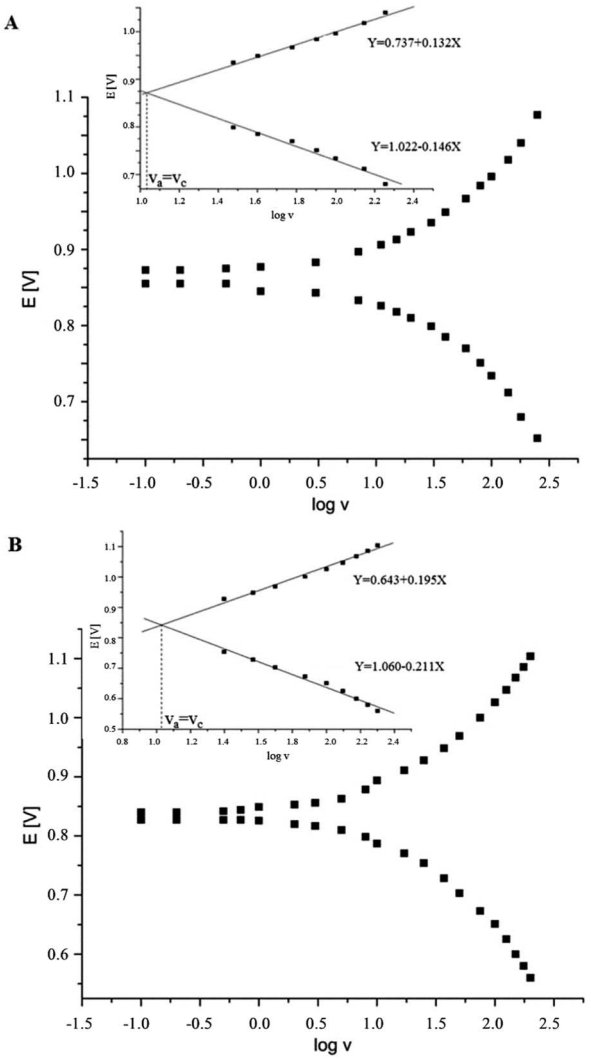

Fig. 6 (A) Voltammetric peak potential *vs.* scan rate dependencies for a gold electrode covered with TEMPO(SH) monolayer and **(B)** TEMPO nanoparticles immobilized on a 1,9-nonanedithiol monolayer. Supporting electrolyte 0.1 M TBAHFP/ACN. Inset: linearized plots for k value determination.

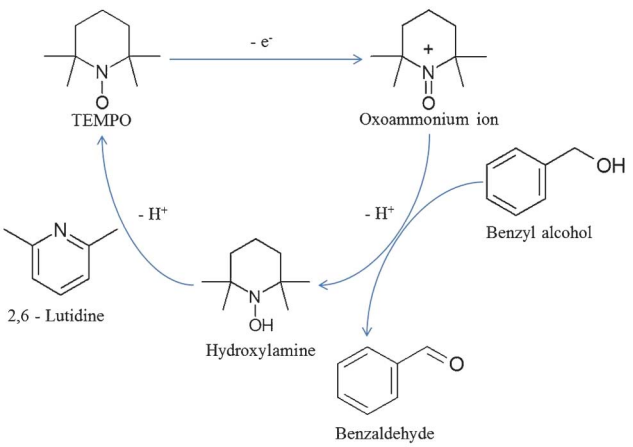

Scheme 3 The scheme of oxidation of benzyl alcohol catalyzed by TEMPO molecules in the presence of 2,6-lutidine.[43]

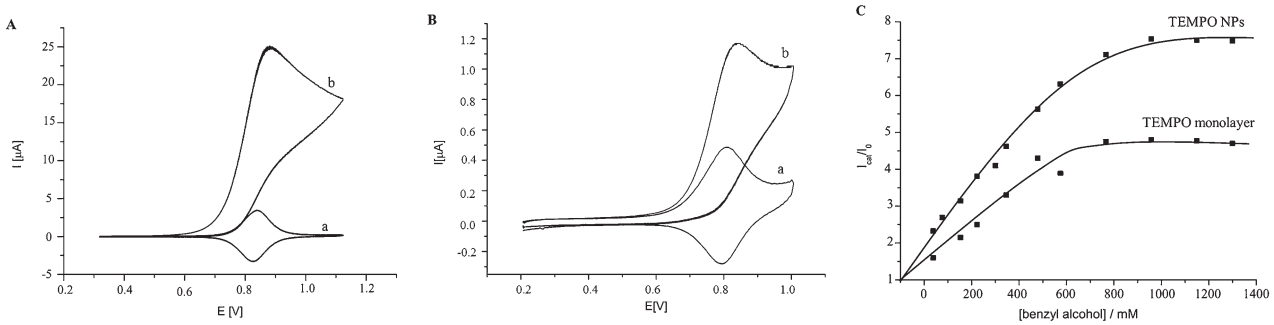

Fig. 7 Cyclic voltammograms of 1,9-nonanedithiol monolayer covered with TEMPO nanoparticles (A) and TEMPO-SH monolayer (B) in 0.1 M TBAHFP in ACN: (a) without and (b) in the presence of benzyl alcohol (580 mM) and 2,6-lutidine (70 mM). (C) The ratio of catalytic peak current to current in the absence of substrate (I_{cat}/I_o) *vs.* concentration of benzyl alcohol for electrocatalytic oxidation of benzyl alcohol using the Au electrode modified by TEMPO nanoparticles and TEMPO-SH monolayer. Scan rate 0.1 V s^{-1}.

located on NPs and the electrode. No special attempts to compensate the IR contribution at high scan rates were made.

3.4 Electrocatalytic oxidation of benzyl alcohol

The catalytic abilities of a TEMPO-nanoparticles modified gold electrode were evaluated by performing experiments in anhydrous ACN containing benzyl alcohol and 2,6-lutidine. The mechanism of oxidation of benzyl alcohol is shown in Scheme 3. 2,6-Lutidine serves as the base, responsible for the regeneration of the free catalyst.[43] Benzyl alcohol and 2,6-lutidine themselves exhibited no voltammetric responses at the bare gold electrode. The voltammogram of the TEMPO-nanoparticles modified gold electrode was not affected by addition of benzyl alcohol.

In the presence of 2,6-lutidine the modified electrode showed typical behavior for the catalytic oxidation of benzyl alcohol to aldehyde (Fig. 7A and 7B). At the nanoparticle covered electrode (Fig. 7A), the peak current corresponding to TEMPO oxidation is larger than in the case of TEMPO-SH monolayer covered surface (Fig. 7B) which reflects the increased number of catalytic sites available for the same geometric area of the working electrode. Moreover, the catalytic abilities of each TEMPO molecule are strengthened for the nanoparticles covered surface since the catalytic current is twenty times larger (Fig. 7A) than recorded using the electrode modified with the monolayer of TEMPO-SH (Fig. 7B). We ascribe the improved catalytic ability to the better accessibility of TEMPO groups attached to the gold nanoparticles than in the case of a closely packed monolayer. The ratio of catalytic peak current (I_c) to catalyst peak current in the absence of benzyl alcohol (I_o), increases with the concentration of benzyl alcohol up to a limiting value. In the plateau region of the plot, the ratio I_c/I_o is 1.63 times larger for the NP-covered surface (Fig. 7C).

4 Conclusion

We show that the population of TEMPO groups on the electrode surface can be significantly increased when TEMPO radicals coated gold nanoparticles form the electrode modifying layer instead of TEMPO-SH molecules. As shown by several methods, the multilayer system containing TEMPO nanoparticles is characterized by high density of the TEMPO groups and their good organization. The kinetics of electron transfer in the two types of TEMPO modified electrodes are comparable. The electrocatalytic oxidation of benzyl alcohol is shown to be more efficient at the electrode surface nanostructured with gold nanoparticles coated with TEMPO radicals than at the electrode modified directly with a monolayer of TEMPO-SH. More importantly, the catalytic efficiency of each TEMPO molecule is found to be larger when the catalyst is immobilized at the nanoparticle surface. We ascribe this improvement to better accessibility of the catalyst at the NP structured electrode compared to that in the well-organized dense TEMPO-SH monolayer. The high value of heterogeneous electron transfer rate constant in the system based on layers of AuNPs modified with TEMPO together with its stability and increased efficiency in oxidizing benzyl alcohol lead us to propose electrodes nanostructured with TEMPO-coated Au nanoparticles as promising surfaces for electrocatalytic applications.

Acknowledgements

This work was supported by Project DEC-2011/01/B/ST5/03941 from the National Science Center.

References

1 T. Vogler and A. Studer, *Synthesis*, 2008, **13**, 1979–1993.
2 A. E. J. De Nooy, A. C. Besemar and H. van Bekkum, *Synthesis*, 1996, **10**, 1153–1174.
3 L. Tebben and A. Studer, *Angew. Chem., Int. Ed.*, 2011, **50**, 5034–5068.
4 R. A. Sheldon and I. W. C. E. Arenas, *Adv. Synth. Catal.*, 2004, **346**, 1051–1071.
5 I. A. Ansari and R. Gree, *Org. Lett.*, 2002, **4**, 1507–1509.
6 R. Criminna and M. Pagliaro, *Org. Process Res. Dev.*, 2010, **14**, 245–251.

7 T. Miyazawa and T. Endo, *J. Polym. Sci. Polym.*, 1985, **23**, 2487–2494.
8 N. Tsubokawa, T. Kimoto and T. Endo, *J. Mol. Catal. A: Chem.*, 1995, **101**, 45–50.
9 D. Brunel, F. Fajula, J.B. Nagy, B. M. Deroide, J. L. Verhoef, J.A. Veum and H. van Bekkum Peters, *Appl. Catal., A*, 2001, **213**, 73–82.
10 Y. Wang, X. Song, S. Shao, H. Zhong and F. Liu, *RSC Adv.*, 2012, **2**, 7693–7698.
11 M. Kuroboshi, K. Goto and H. Tanaka, *Synthesis*, 2008, **6**, 903.
12 H. Tanaka, Y. Kawakami, K. Goto and M. Kuroboshi, *Tetrahedron Lett.*, 2001, **42**, 445–448.
13 S. Kishioka, S. Ohki, T. Ohsaka and K. Tokuda, *J. Electroanal. Chem.*, 1998, **452**, 179–186.
14 D. Astruc, F. Lu and J. R. Aranzaes, *Angew. Chem., Int. Ed.*, 2005, **44**, 7852–7872 and references therein.
15 L. Pasquato, P. Pengo and P. Scrimin, *J. Mater. Chem.*, 2004, **14**, 3481–3487.
16 E. C. Dreaden, A. M. Alkilany, X. Huang, C. J. Murphy and M. A. El-Sayed, *Chem. Soc. Rev.*, 2012, **41**, 2740–2779 and references therein.
17 J. Turkevitch, P. C. Stevenson and J. Hillier, *Discuss. Faraday Soc.*, 1951, **11**, 55–75.
18 M. Brust, M. Walker, D. Bethell, D. J. Schiffrin and R. Whyman, *J. Chem. Soc., Chem. Commun.*, 1994, 801–802.
19 M.-Ch. Daniel and D. Astruc, *Chem. Rev.*, 2004, **104**, 293–346.
20 L. A. Porter, D. Ji, S. L. Westcott, M. Graupe, R. S. Czernuszewicz, N. J. Halas and T. R. Lee, *Langmuir*, 1998, **14**, 7378–7386.
21 H. A. Biebuyck, C. D. Bain and G. M. Whitesides, *Langmuir*, 1994, **10**, 1825–1831.
22 P. Ionita, A. Caragheorgheopol, B. C. Gilbert and V. Chechik, *J. Am. Chem. Soc.*, 2002, **124**, 9048–9049.
23 H. Schőnherr and H. Ringsdorf, *Langmuir*, 1996, **12**, 3891–3897.
24 A. C. Templeton, M. J. Hostetler, E. K. Warmoth, S. Chen, C. M. Hartshorn, V. M. Krishnamurthy, M. D. E. Forbes and R. W. Murray, *J. Am. Chem. Soc.*, 1998, **120**, 4845–4849.
25 V. Chechik, H. J. Wellsted, A. Korte, B. C. Gilbert, H. Caldararu, P. Ionita and A. Caragheorgheopol, *Faraday Discuss.*, 2004, **125**, 279–290.
26 M. J. Hostetler, A. C. Templeton and R. W. Murray, *Langmuir*, 1999, **15**, 3782–3789.
27 C. A. Waters, A. J. Mills, K. A. Johnson and D. J. Schiffrin, *Chem. Commun.*, 2003, 540–541.
28 S. H. Chen and K. Kimura, *Langmuir*, 1999, **15**, 1075–1082.
29 A. C. Templeton, S. W. Chen, S. M. Gross and R. W. Murray, *Langmuir*, 1999, **15**, 66–76.
30 C. K. Yee, R. Jordan, A. Ulman, H. White, A. King, M. Rafailovich and J. Sokolov, *Langmuir*, 1999, **15**, 3486–3491.
31 M. P. Rowe, K. E. Plass, K. Kim, C. Kurdak, E. T. Zellers and A. J. Matzger, *Chem. Mater.*, 2004, **16**, 3513–3517.
32 P. J. Roth and P. Theato, *Chem. Mater.*, 2008, **20**, 1614–1621.
33 A. Schätz, R. N. Grass, W. J. Stark and O. Reiser, *Chem.–Eur. J.*, 2008, **14**, 8262–8266.
34 O. Swiech, N. Hrynkiewicz-Sudnik, B. Palys, A. Kaim and R. Bilewicz, *J. Phys. Chem. C*, 2011, **115**, 7347–7354.
35 S. Kishioka, S. Ohki, T. Ohsaka and K. Tokuda, *J. Electroanal. Chem.*, 1998, **452**, 179–186.
36 R. Nicolay, L. Marx, P. Hemery and K. Matyjaszewski, *Macromolecules*, 2007, **40**, 9217–9223.
37 J. P. Hoare, *J. Electrochem. Soc.*, 1984, **131**, 1808–1815.
38 H. Casselas, D. De Caro, L. Valade and J. Fraxedas, *New J. Chem.*, 2002, **26**, 915–919.
39 J. Caro, J. Fraxedas, O. Jürgens, J. Santiso, C. Rovira, J. Veciana and A. Figueras, *Adv. Mater.*, 1998, **10**, 608–610.
40 J. Fraxedas, J. Caro, A. Figueras, P. Gorostiza and F. Sanz, *J. Vac. Sci. Technol., A*, 1998, **16**, 2517–2523.
41 E. Laviron, *J. Electroanal. Chem.*, 1979, **101**, 19–28.
42 H. Daifuku, K. Aoki, K. Tokuda and H. Matsuda, *J. Electroanal. Chem.*, 1985, **183**, 1–26.
43 O. Onamura, in *''The Chemistry of Hydroxylamines, Oximes and Hydroxamic Acids''*, John Wiley & Sons, 2009, vol. 1 ch. 10 pp. 499–506.

